Stress-induced ferroelectricity and soft phonon modes in $SrTiO_3$

Hiromoto Uwe* and Tunetaro Sakudo
Electrotechnical Laboratory, Tanashi, Tokyo, Japan
(Received 3 March 1975)

By means of dielectric measurements and a Raman-scattering experiment, the uniaxial stress dependence of the ferroelectric and structural phonon modes in $SrTiO_3$ crystal has been studied at liquid-helium temperature. The ferroelectric phase transitions were induced by a stress normal to the (100) or (110) face. The inverse dielectric susceptibilities were found to change linearly with applied stress, and the phonon frequencies of corresponding ferroelectric modes were found to vary following the Lyddane-Sachs-Teller relation. These characteristics were analyzed by using the phenomenological free energy which contains as interaction terms $Q_{\lambda\mu}X_\lambda(\vec{P}\vec{P})_\mu + R_{\lambda\mu}X_\lambda(\vec{\Phi}\vec{\Phi})_\mu + t_{\lambda\mu}(\vec{P}\vec{P})_\lambda(\vec{\Phi}\vec{\Phi})_\mu$. From the behavior of the dielectric constants below the critical stress and that of the soft-phonon-mode frequencies above the critical stress, the coupling coefficients $Q_{\lambda\mu}$, $R_{\lambda\mu}$, $t_{\lambda\mu}$ and other parameters in the free energy have been determined consistently. Anticrossing between the ferroelectric and structural modes was observed for an oblique-wave-vector phonon. Anomalous increase of the damping of the total symmetric ferroelectric mode near the transition stress has been found and discussed.

I. INTRODUCTION

$SrTiO_3$ crystal has been a convenient stage for the lattice-dynamical study of the displacive phase transitions, involving both ferroelectric and structural ones. In this crystal, the F_{2u} (Γ_{25}) zone-boundary phonon mode condenses at $T_a = 105$ K and the structural phase transition from O_h to D_{4h} takes place.[1-4] On the other hand, the F_{1u} (Γ_{15}) zone-center phonon mode responsible for the ferroelectric (FE) transformation has been found not to condense at any temperature. When the temperature is lowered the dielectric constant increases by as much as 10^4 in the liquid-He temperature range.[5,6] However, deviation from the Curie-Weiss behavior is manifest below about 60 K, which is understood as due to a quantum effect of the polarizabilities of constituent ions in the crystal,[7] or the stabilization of the bare phonon by the phonon cloud owing to zero-point fluctuations.[8] Characteristics of the FE phonon mode have been directly observed by means of neutron inelastic scattering[9] and electric-field-induced Raman scattering[10] to demonstrate that the phonon frequency at $k = 0$ varies with temperature following the Lyddane-Sachs-Teller (LST) relation and the phonon mode indeed tends toward but never reaches zero frequency on cooling. This highly polarizable state due to the lingering soft FE mode is conventionally called as "incipient ferroelectric" state.

Recently, it has become well recognized that external pressure, either hydrostatic or uniaxial, is a useful variable in the study of the properties of phase transitions due to lattice instabilities. Hydrostatic-pressure experiments have shown, generally for the displacive transition, that the ferroelectric transition temperature decreases, whereas the structural transition temperature increases with decreasing lattice volume.[11] As for the uniaxial stress effect for the dielectrics, Burke and Pressley[12] have found in fluorescence spectra of the Cr^{3+}-doped crystal that uniaxial stress applied to a (111) face can produce a pressure-induced structural transition from tetragonal to trigonal symmetry. Raman[13-15] and ESR[16] studies on the pressure-induced change of the relevant soft phonon mode and the spontaneous order parameter were made and compared with a phenomenological theory.[17] Next, Burke and Pressley have found in their dielectric observation[18] that the ferroelectric phase can also be induced by applying mechanical stress above some critical values along the pseudocubic ⟨100⟩ or ⟨110⟩ direction. Evidence of the stress-induced piezoelectricity above the critical stress was provided by the optical-second-harmonic generation experiment.[19] Stress-induced ferroelectricity was also found in the case of $KTaO_3$, which is also incipient ferroelectric.[20,21]

Properties of the displacive phase transitions can generally be analyzed by the phenomenological theory employing a thermodynamical free energy,[4,17,21,22] though the situation is rather complicated in the case of $SrTiO_3$ at low temperatures because the two kinds of soft phonon modes coexist in this crystal. That is, the two kinds of order

parameter, one represented by the polarization P_i and the other one by the rotation of oxygen octahedra Φ_i, should be involved in the free energy. Interaction between them and also with the lattice strain x_{ij} must be taken into account.

In this report we present the study of the pressure behavior of these soft phonon modes in $SrTiO_3$ under a stress normal to the (100) or (110) face, at liquid-He temperatures, by means of dielectric measurements and a Raman-scattering experiment. It will be shown that stress-induced ferroelectricity can be understood as due to the electrostrictive effect in the incipient ferroelectric crystal, and that the FE mode frequency varies with stress toward zero value as expected, but with the characteristic divergence of the damping constant of the mode as the transition stress is approached. Comparing the experimental results with a phenomenological theory based on the free energy which contains P_i, Φ_i, and x_{ij} as arguments, we can obtain a self-consistent set of coefficients for the crystal. Employing the uniaxial stress as an external variable seems to be indispensable for determining separately these many coupling parameters which appear in the free energy.

II. PHENOMENOLOGICAL THEORY

A. Free energy

As mentioned above, the free energy we are going to deal with should involve the three different sets of thermodynamic variables: the electric polarization P_i and the magnitude of the staggered rotation of oxygen octahedra Φ_i which correspond, respectively, to the amplitudes of the two soft phonon modes F_{1u} and F_{2u} in the crystal, and an additional variable which represents the lattice strain x_{ij} or stress X_{ij}. We write the Helmholtz free energy $A(P_i, \Phi_i, x_{ij})$ per unit crystal volume as follows:

$$A = \tfrac{1}{2}\gamma_0 \sum_i P_i^2 + D^x\Big(\sum_i P_i^2\Big)^2 + \tfrac{1}{2} D_n^x \sum_{i\neq j} P_i^2 P_j^2 + \tfrac{1}{2}\kappa_0 \sum_i \Phi_i^2 + A^x\Big(\sum_i \Phi_i^2\Big)^2 + \tfrac{1}{2} A_n^x \sum_{i\neq j} \Phi_i^2 \Phi_j^2$$
$$+ \tfrac{1}{2}\sum_{ijkl} c_{ijkl} x_{ij} x_{kl} - \sum_{ijkl} (g_{ijkl} x_{ij} P_k P_l + b_{ijkl} x_{ij} \Phi_k \Phi_l + t^x_{ijkl} P_i P_j \Phi_k \Phi_l) , \quad (1)$$

where i, j, k, and $l = 1$, 2, and 3 are referred to the pseudocubic axes. The coefficients in Eq. (1) are generally regarded as insensitive to temperature except those of the quadratic term, γ_0 and κ_0: γ_0 should vary as $T - T_C$ with $T_C \simeq 31$ K and κ_0 as $T - T_a$ with $T_a \simeq 105$ K. However, owing to the quantum effect mentioned in Sec. I, the inverse dielectric susceptibility γ_0 becomes almost constant over the liquid-He temperature range we are concerned with in the present experiment.[6] The value of γ_0 is unusually small as implied by the incipient ferroelectric nature. The form of the fourth rank tensors appearing in Eq. (1) is dictated by the symmetry consideration.[23] Since the high-temperature phase of the crystal is of point symmetry O_h, the nonvanishing elements of the fourth rank tensors are, in the contracted notation for the suffix, (11), (12) and (44) components. The condition that $b_{11} + 2b_{12} = 0$,[17,22] is not adopted in this paper.

In order to deal with the physical quantities under the condition of variable external stress, it is more convenient to employ the Gibbs free energy G which involves, other than P_i and Φ_i, stress components X_{ij} instead of x_{ij}. The elastic Gibbs function for $T > T_a$, G^c, can be derived as follows. By minimizing $A - \sum_\lambda x_\lambda X_\lambda$ with respect to x_λ, one gets equilibrium values of x_λ. They are, for instance,

$$\bar{x}_1 = [X_1 + X_2 + X_3 + (g_{11} + 2g_{12}) P^2 + (b_{11} + 2b_{12})\Phi^2]/3(c_{11} + 2c_{12})$$
$$+ [2X_1 - X_2 - X_3 + (g_{11} - g_{12})(2P_1^2 - P_2^2 - P_3^2) + (b_{11} - b_{12})(2\Phi_1^2 - \Phi_2^2 - \Phi_3^2)]/3(c_{11} - c_{12}) , \quad (2)$$
$$\bar{x}_4 = (X_4 + g_{44} P_2 P_3 + b_{44}\Phi_2\Phi_3)/c_{44} .$$

Putting $\bar{x}_\lambda$ into $A - \sum_\lambda x_\lambda X_\lambda$, we obtain the free energy as a function of P_i, Φ_i, and X_λ as follows:

$$G^c = \tfrac{1}{2}\gamma_0 \sum_i P_i^2 + D^X \Big(\sum_i P_i^2 \Big)^2 + \tfrac{1}{2} D_n^X \sum_{i \neq j} P_i^2 P_j^2$$
$$+ \tfrac{1}{2}\kappa_0 \sum_i \Phi_i^2 + A^X \Big(\sum_i \Phi_i^2 \Big)^2 + \tfrac{1}{2} A_n^X \sum_{i \neq j} \Phi_i^2 \Phi_j^2 + \tfrac{1}{2} \sum S_{ijkl} X_{ij} X_{kl}$$
$$- \sum (Q_{ijkl}^c X_{ij} P_k P_l + R_{ijkl} X_{ij} \Phi_k \Phi_l + t_{ijkl}^X P_i P_j \Phi_k \Phi_l) \ . \tag{3}$$

The superscripts x and X indicate that the symbols stand for the coefficients under the condition of constant strain and constant stress, respectively. The superscripts c and t mean that the symbols refer to those of the cubic and the tetragonal state. The relations between the corresponding parameters in A and G^c are given in the Appendix.

The equilibrium value of the structural order parameter $\bar{\Phi}_i$ is given by solving the equations

$$\left. \frac{\partial G^c}{\partial \Phi_i} \right|_{\Phi_i = \bar{\Phi}_i} = 0 \quad (i = 1, 2, 3) \ . \tag{4}$$

The cubic state ($\bar{\Phi}_i = 0$) is no more stable below T_a as $\kappa_0 < 0$. For $SrTiO_3$ under free stress, the tetragonal state with $\bar{\Phi}_i = (0, 0, \pm\Phi_s)$ is known to be stable, because $A_n^X > 0$, with the spontaneous value

$$\Phi_s = (-\kappa_0 / 4A^X)^{1/2} \ . \tag{5}$$

In the presence of applied stress and/or electric polarization, it is not generally possible to get the analytical solution of Eq. (4). However, if we assume that (a) $X_4 = X_5 = 0$, which is valid for a stress normal to the (010) or (110) face, and (b) $\bar{\Phi}_3 \gg \bar{\Phi}_1, \bar{\Phi}_2$, we may put $t_{44}^X = 0$ in G^c for solving Eq. (4). Then, we get an approximate solution as follows:

$$\bar{\Phi}_1 = \bar{\Phi}_2 = 0 \ ,$$
$$\bar{\Phi}_3^2 = \Phi_s^2 + [R_{12}(X_1 + X_2) + R_{11} X_3 + t_{12}^X (P_1^2 + P_2^2) + t_{11}^X P_3^2] (2A^X)^{-1} \ . \tag{6}$$

Substituting these $\bar{\Phi}_i$ values into Eq. (3) we obtain as the Gibbs function G^t to be used in the tetragonal phase the following form:

$$G^t = G_0^t + \tfrac{1}{2}\gamma_a (P_1^2 + P_2^2) + \tfrac{1}{2}\gamma_c P_3^2 + D^X \Big(\sum_i P_i^2 \Big)^2 + \tfrac{1}{2} D_n^X \sum_{i \neq j} P_i^2 P_j^2 - (4A^X)^{-1} [t_{12}^X (P_1^2 + P_2^2) + t_{11}^X P_3^2]^2$$
$$- (Q_{11}^t X_1 + Q_{12}^t X_2 + Q_{31}^t X_3) P_1^2 - (Q_{12}^t X_1 + Q_{11}^t X_2 + Q_{31}^t X_3) P_2^2 - [Q_{13}^t (X_1 + X_2) + Q_{33}^t X_3] P_3^2 - Q_{66}^t X_6 P_1 P_2 \ , \tag{7}$$

where

$$\gamma_a = \gamma_0 - 2 t_{12}^X \Phi_s^2 \ ,$$
$$\gamma_c = \gamma_0 - 2 t_{11}^X \Phi_s^2 \ , \tag{8}$$

and the realtions between $Q_{\lambda\mu}^t$ and $Q_{\lambda\mu}^c$ are as follows:

$$Q_{11,12}^t = Q_{11,12}^c + (R_{12} t_{12}^X)/2A^X \ ,$$
$$Q_{13}^t = Q_{12}^c + (R_{12} t_{11}^X)/2A^X \ ,$$
$$Q_{31}^t = Q_{12}^c + (R_{11} t_{12}^X)/2A^X \ , \tag{9}$$
$$Q_{33}^t = Q_{11}^c + (R_{11} t_{12}^X)/2A^X \ ,$$
$$Q_{66}^t = Q_{44}^c \ .$$

B. Dielectric susceptibilities

A set of dielectric constants ϵ_i along the principal directions is derived for the "free" crystal state from the Gibbs function by the relation

$$\epsilon_i = 4\pi\gamma_i^{-1} + 1 \ ,$$

$$\gamma_i = \left. \frac{\partial^2 G^{c,t}}{\partial \hat{P}_i^2} \right|_{eq} \quad (i = 1, 2, 3) \ , \tag{10}$$

where γ_i denotes the inverse dielectric susceptibility and $\hat{P}_i$ stands for the component of the electric polarization along the principal axis of the dielectric tensor concerned. It is readily seen from Eq. (7) that for crystals without the external stress and below T_a,

$$\{\gamma_i\} = (\gamma_a, \gamma_a, \gamma_c) \ , \tag{11}$$

with $\hat{P}_i$ along the $\langle 100 \rangle$ directions. In passing, we note that the dielectric anisotropy in Eq. (11) originates from the interactions of the structural order parameter Φ_i not only with the electric polarization but also with the lattice strain [see Eq. (A4)]. In the following, we will focus our attention to the cases of the tetragonal phase and of the uniaxial stress applied normal to the pseudocubic (010) or (110) planes. Hereafter, we designate them as the (010) or (110) stress.

1. (010) stress

In this case, the principal axes of the dielectric tensor are along the pseudocubic ⟨100⟩ axes. For convenience, we take the directions of stress and tetrad c axes, respectively, along the 2 and 3 axes, i.e., $X_2 = -\sigma$ and other X_i equal to zero, where σ represents the magnitude of the uniaxial compressional stress per unit area. Furthermore, we employ the notation x, y, z instead of 1, 2, 3 for the suffix of γ. Then, from Eqs. (7) and (10) we find

$$\begin{aligned} \gamma_x &= \gamma_a + 2Q_{12}^t \sigma \ , \\ \gamma_y &= \gamma_a + 2Q_{11}^t \sigma \ , \\ \gamma_z &= \gamma_c + 2Q_{13}^t \sigma \ . \end{aligned} \tag{12}$$

These equations indicate that the electrostrictive constants can be known from the slope of $\Delta\gamma/\Delta\sigma$. From experimental observations described below, we find $Q_{12}^t, Q_{13}^t < 0$ for this crystal. Then, Eq. (12) may predict that the vanishing of γ_i, or the induced ferroelectric phase transition, should take place at the critical stresses

$$\sigma_{c1} \equiv -\gamma_a/2Q_{12}^t, \quad \sigma_{c2} \equiv -\gamma_c/2Q_{13}^t \ . \tag{13}$$

Experimental observations indicate that $\sigma_{c1} < \sigma_{c2}$. Then, we expect that γ_x will vanish at $\sigma = \sigma_{c1}$ and the spontaneous polarization P_{s1} will develop in the direction perpendicular to both the stress and the structural tetrad axes. The magnitude of P_{s1} will vary as

$$P_{s1}^2 = -\tfrac{1}{2} Q_{12}^t [D^X - (t_{12}^X)^2/4A^X]^{-1} (\sigma - \sigma_{c1}) \ . \tag{14}$$

In the ferroelectric phase, the dielectric susceptibilities are expected to vary as

$$\begin{aligned} \gamma_x &= -2(\gamma_a + 2Q_{12}^t \sigma), \\ \gamma_y &= \gamma_a + 2Q_{11}^t \sigma + [4D^X + 2D_n^X - (t_{12}^X)^2/A^X] P_{s1}^2, \\ \gamma_z &= \gamma_c + 2Q_{13}^t \sigma + (4D^X + 2D_n^X - t_{11}^X t_{12}^X/A^X) P_{s1}^2. \end{aligned} \tag{15}$$

2. (110) stress

When the uniaxial stress is applied normal to the (110) face, $X_1 = X_2 = X_6 = -\frac{1}{2}\sigma$ and others are equal to zero. In this case, $\hat{P}_1$, $\hat{P}_2$, and $\hat{P}_3$ have to be taken respectively along $[1\bar{1}0]$, $[110]$, and $[001]$, which we denote by an X, Y, Z suffix on γ. Then, from Eqs. (7) and (10), we find

$$\begin{aligned} \gamma_X &= \gamma_a + (Q_{11}^t + Q_{12}^t - \tfrac{1}{2}Q_{66}^t)\sigma, \\ \gamma_Y &= \gamma_a + (Q_{11}^t + Q_{12}^t + \tfrac{1}{2}Q_{66}^t)\sigma, \\ \gamma_Z &= \gamma_c + 2Q_{13}^t \sigma. \end{aligned} \tag{16}$$

The induced ferroelectric transition is expected to occur along the Z direction (parallel to the structural c axis) at the critical stress σ_{c2} of Eq. (13). For $\sigma > \sigma_{c2}$, the spontaneous polarization P_{s2} along $[001]$ should vary as

$$P_{s2}^2 = -\tfrac{1}{2} Q_{13}^t [D^X - (t_{11}^X)^2/4A^X]^{-1} (\sigma - \sigma_{c2}), \tag{17}$$

and the dielectric susceptibilities vary in the ferroelectric phase as

$$\begin{aligned} \gamma_{X,Y} &= \gamma_{X,Y}(\sigma < \sigma_{c2}) \\ &\quad + (4D^X + 2D_n^X - t_{11}^X t_{12}^X/A^X) P_{s2}^2, \\ \gamma_Z &= -2(\gamma_c + 2Q_{13}^t \sigma). \end{aligned} \tag{18}$$

Experimental observations indicate that $Q_{11}^t + Q_{12}^t \pm \frac{1}{2}Q_{66}^t > 0$, which guarantees that the above solution is unique.

C. Soft-mode frequencies

The ferroelectric and the structural soft modes can be regarded as the vibrations of the relevant normal-mode coordinates around their equilibrium points determined above. These phonon frequencies, Ω_{P_i} and Ω_{Φ_i} are given by the equations

$$\begin{aligned} m_P \left(\frac{v}{e^*}\right)^2 \Omega_{P_i}^2 &= \left.\frac{\partial^2 A}{\partial \hat{P}_i^2}\right|_{\text{eq}} , \\ m_\Phi \Omega_{\Phi_i}^2 &= \left.\frac{\partial^2 A}{\partial \Phi_i^2}\right|_{\text{eq}} , \end{aligned} \tag{19}$$

where m_P and m_Φ stand for mass densities of the corresponding modes, e^* is an effictive charge, and v is the unit-cell volume. Equation (19) should be evaluated at the equilibrium point, $x_\lambda = \bar{x}_\lambda$, $\Phi_i = \bar{\Phi}_i$, and $P_i = \bar{P}_i$, using Eqs. (2), (6), and (14) or (17). Since the *homogeneous* strain oscillation can generally not follow the *internal* strain oscillation, the Helmholtz function A, instead of G, should appear in Eq. (19). Here, it is to be noted that: (a) the equation indicates that the square of the ferroelectric mode frequency $\Omega_{P_i}^2$, should be proportional to the inverse dielectric susceptibilities in the clamped state, which are the same as those in the free state for $\sigma < \sigma_c$; (b) the statement in (a) implies, in view of the LST relation which involves all the ir-active phonon branches, that Eq. (19) postulates the invariance of the phonon frequencies of ir-active modes other than the ferroelectric one. This was experimentally verified, as described below. (c) In the stress-induced ferroelectric phase where both P_s and Φ_s coexist, a coupling between the ferroelectric and the structural modes may arise owing to a bilinear coupling with a coefficient $t_{\lambda\mu}^x P_s \Phi_s$. The example will be shown in Sec. V B.

Irreducible representations of both ferroelectric and structural phonon modes under various conditions are summarized in Table I. For instance, low-lying infrared-active F_{1u}-mode (triply-degenerate) in the cubic perovskite lattice (O_h^1) de-

TABLE I. Correlation table for soft phonon modes.

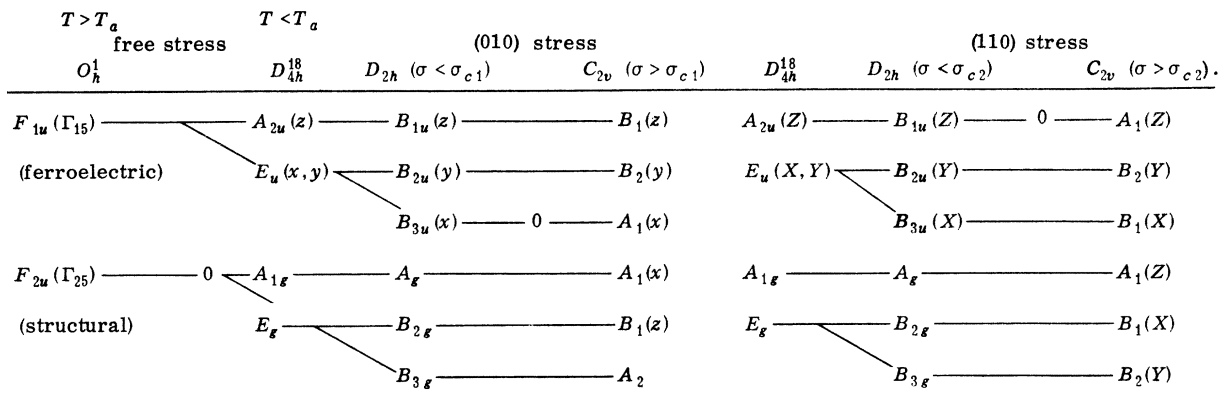

composes in the tetragonal phase below T_a (D_{4h}^{18}) into the A_{2u} and E_u modes. Under the (100) stress, the crystal symmetry changes from D_{4h} into D_{2h}, and the E_u mode splits into nondegenerate B_{2u} and B_{3u} modes, the latter of which condenses at the critical stress σ_{c1} and becomes the A_1 mode of the induced ferroelectric phase (C_{2v}). Straightforward calculations using Eq. (19) lead to the following expression for the respective phonon frequencies.

1. Free stress

Both A_{2u} and E_u modes remain Raman inactive for the D_{4h} and the D_{2h} states until the crystal becomes piezoelectric in the C_{2v} state. On the other hand, the E_g and the A_{1g} modes, which stemmed from the F_{2u} mode, become Raman active in the tetragonal phase below $T_a = 105$ K. We find

$$\begin{aligned} &m_P(v/e^*)^2\Omega_P^2(E_u)=\gamma_a,\\ &m_P(v/e^*)^2\Omega_P^2(A_{2u})=\gamma_c,\\ &m_\Phi\Omega_\Phi^2(E_g)=-\kappa_0(2A_n^X+b_{44}^2/c_{44})/4A^X,\\ &m_\Phi\Omega_\Phi^2(A_{1g})=-2\kappa_0 A^x/A^X. \end{aligned} \tag{20}$$

2. (010) stress

$$\begin{aligned} &m_P(v/e^*)^2\Omega_P^2(B_{3u}-A_1)=\begin{cases}\gamma_x, & \sigma<\sigma_{c1}\\ 8D^x P_{s1}^2, & \sigma>\sigma_{c1}\end{cases}\\ &m_P(v/e^*)^2\Omega_P^2(B_{2u}-B_2)=\gamma_y+(g_{44}^2/c_{44})P_{s1}^2,\\ &m_P(v/e^*)^2\Omega_P^2(B_{1u}-B_1)=\gamma_z+(g_{44}^2/c_{44})P_{s1}^2. \end{aligned} \tag{21}$$

It is to be noted in Eqs. (21) that the contributions proportional to P_{s1}^2 ($\propto\sigma-\sigma_{c1}$) also come from γ_i [cf. Eq. (15)]. The expression for Ω_Φ^2 to be shown below is apparently complicated by the presence of the correction term proportional to P_{s1}^2 which, however, proved to be negligibly small by the observation.

$$\begin{aligned} m_\Phi\Omega_{\Phi_1}^2(B_{2g}-B_1)&=-(\kappa_0+2R_{12}\sigma)(2A_n^X+b_{44}^2/c_{44})/4A^X\\ &\quad-2[t_{11}^X-t_{12}^X\\ &\quad-(2A_n^X+b_{44}^2/c_{44})(t_{11}^X/4A^X)]P_{s1}^2,\\ m_\Phi\Omega_{\Phi_2}^2(B_{3g}-A_2)&=m_\Phi\Omega_{\Phi_1}^2(B_{2g}-B_1)+2(R_{11}-R_{12})\sigma\\ &\quad+(2A_n^X+b_{44}^2/c_{44})(t_{12}^X/2A^X)P_{s1}^2,\\ m_\Phi\Omega_{\Phi_3}^2(A_g-A_1)&=-(2A^x/A^X)\kappa_0-4R_{12}\sigma\\ &\quad+(4A^x t_{12}^X/A^X)P_{s1}^2. \end{aligned} \tag{22}$$

3. (110) stress

$$m_P(v/e^*)^2\Omega_P^2(B_{1u}-A_1)=\begin{cases}\gamma_Z, & \sigma<\sigma_{c2}\\ 8D^X P_{s2}^2, & \sigma>\sigma_{c2}\end{cases} \tag{23}$$

$$\begin{aligned} &m_P(v/e^*)^2\Omega_P^2(B_{3u}-B_1)=\gamma_X+(g_{44}^2/c_{44})P_{s2}^2,\\ &m_P(v/e^*)^2\Omega_P^2(B_{2u}-B_2)=\gamma_Y+(g_{44}^2/c_{44})P_{s2}^2,\\ &m_\Phi\Omega_{\Phi_X}^2(B_{2g}-B_1)=m_\Phi\Omega_\Phi^2(E_g)+\Delta_-(\sigma,P_{s2}),\\ &m_\Phi\Omega_{\Phi_Y}^2(B_{3g}-B_2)=m_\Phi\Omega_\Phi^2(E_g)+\Delta_+(\sigma,P_{s2}), \end{aligned} \tag{24}$$

$$\begin{aligned} m_\Phi\Omega_{\Phi_Z}^2(A_g-A_1)&=m_\Phi\Omega_\Phi^2(A_{1g})-4(A^x/A^X)R_{12}\sigma\\ &\quad+4(A^x/A^X)t_{11}^X P_{s2}^2, \end{aligned}$$

where

$$\begin{aligned} \Delta_\mp(\sigma,P_{s2})&=[R_{11}-R_{12}(2A^X+2A_n^X+b_{44}^2/c_{44})/2A^X\mp\tfrac{1}{2}R_{44}]\sigma\\ &\quad+[(4A^X+2A_n^X+b_{44}^2/c_{44})t_{11}^X/2A^X-2t_{12}^X]P_{s2}^2. \end{aligned}$$

III. EXPERIMENTAL

$SrTiO_3$ crystals grown by the flame-fusion method were supplied from the Nakazumi Crystals

Corp. Samples were cut from the boules in a parallelepiped with (100) or (110) faces, typically $1.5\times2\times7$ mm^3 in size, with a stress being applied along the 7-mm dimension. For the experiment on the compressive-stress effect, care has to be taken to reduce the inhomogeneity of the stress in the sample and to prevent the fracture of samples under heavy stress. End planes to be pressed were polished as accurately parallel as possible, and stress was applied to the sample via thin sapphire disks which were glued with epoxy resin. This procedure proved to be effective against the fracture of samples. As an inhomogeneous stress was expected to be localized near the pressed faces, we contrived to observe only the middle part of the long sample where a good homogeneous stress was ensured.[21]

The dielectric constant was measured with a capacitance bridge which employed the three-terminal method at frequencies of 1–100 kHz far below the mechanical resonance frequencies of samples. Figure 1 shows the experimental arrangement for the Raman-scattering measurement. Linearly polarized light of 0.3 W at 4880 Å from an Ar^+ laser was focused into the sample sandwiched between the pressing blocks in the optical Dewar. By rotating a half-wavelength plate and an analyzer, four components of the Raman-scattering tensor were examined. The 90°-angle scattered light passed through a Dove prism and was focused on the slit plane of a double monochromator (Spex, Model 1401), which was followed by a photomultiplier (EMI-6256S, dry-ice cooled) and a photon counting circuit (dark current: 10 counts/sec). As shown in Fig. 1, the length of the slit was adjusted so that the image of the illuminated surfaces of the sample was out of the slit, which served to reduce stray scattering light. Slit widths were chosen as narrow as 0.5–2 cm^{-1}. This optical arrangement limited the observed scattering volume to a region (0.1 mm diam$\times$1 mm), which was much smaller than the whole specimen ($2\times1.5\times7$ mm^3). This enabled us to prevent the effect of the inhomogeneity of the stress.

The magnitude of the applied stress was measured by the calibrated strain gauge in a load cell (Baldwin-Lima-Hamilton Electronics, Inc., sensitivity: 10^{-9} V/dyn) placed at the opposite side of the lever.

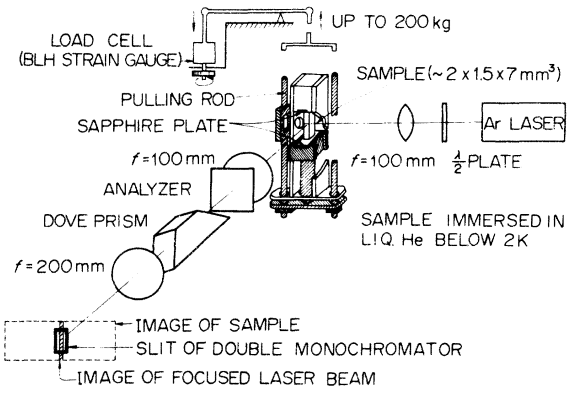

FIG. 1. Experimental arrangement of the Raman scattering for application of stress. Shaded parts of the sample holder are movable and connected to one end of the lever through which the stress load is applied.

IV. DIELECTRIC MEASUREMENT

In the low-temperature phase, the crystal becomes comprised of multiple domains with the c axis oriented along one of the different ⟨100⟩ directions. The boundaries of these structural domains can be moved by an external stress in such a way that the domains whose c axes are mostly perpendicular to the applied compressive stress expand at the expense of domains with unfavorable c directions.[24,25] By using this effect, anisotropic dielectric susceptibilities below T_a were also measured as a function of temperature for the stress-treated crystals.[6] The previous measurement of the stress-induced dielectric anomaly for the case of the (010) stress was not free from the ambiguity due to the presence of multidomains.[18] A similar experiment on $KTaO_3$ provided us with a simpler example, since in this case there is no am-

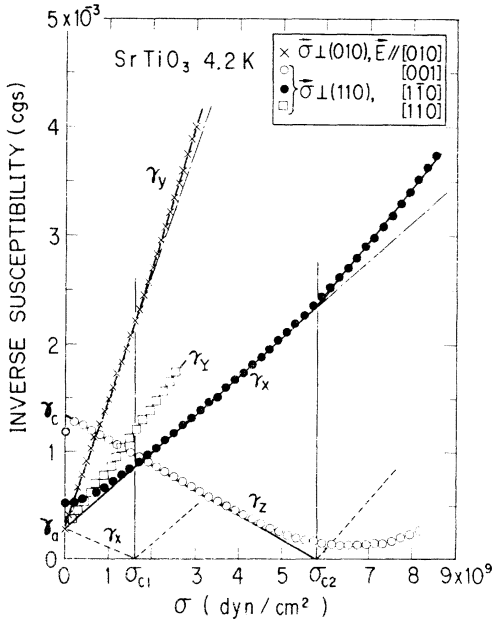

FIG. 2. Inverse dielectric susceptibilities vs stess load σ for $SrTiO_3$ at 4.2 K. γ_x and γ_y are for the (010) stress, and γ_X, γ_Y, and γ_Z for the (110) stress. Broken lines for γ_X and γ_Z are theoretical ones (see the text).

biguity due to the structural domain.[20,21] In the case of both crystals, however, the observation of the spontaneous polarization in the induced ferroelectric phase was unsuccessful, as the stressed crystals can exhibit only a rounded hysteresis loop even far above the critical stress.[18,20]

In the present study, we have extended the observation of the stress-induced change in the dielectric constants of $SrTiO_3$, paying attention to the lateral effect as to the ferroelectric direction. The observed characteristics are summarized in Fig. 2 which is the plot of the inverse susceptibilities γ_i versus the stress value σ. In this figure one notes that most γ_i's vary in general linearly with σ up to the critical stress where the γ_i for polar directions show minima and the ones for lateral directions exhibit upward kinks. These features are in accord with the theory described in Sec. II B. On closer inspection of the figure, however, one notes the following points: (a) Departure from the linear relationship is observed in the lower-stress region. This is probably due to the domain-reorientation process. The lines extrapolated from the higher-σ region converge to either γ_a or γ_c at zero stress [see Eqs. (8), (12), and (16)]. The ratio of $\gamma_c/\gamma_a \sim 4$ ($\epsilon_a = 41\,900$, $\epsilon_c = 9380$) is appreciably larger by a factor of 2 than the one previously reported.[6] (b) For both the (010) and (110) stresses, the values of the critical stress corresponding to the minima in the polar directions [0.99×10^9 dyn-cm^2 for the (010) stress[18] and 6.6×10^9 dyn/cm^2 for the (110) stress] are substantially different from those corresponding to the kinks in the lateral directions [$(1.6\pm0.2)\times10^9$ dyn/cm^2 for the (010) stress and $(5.8\pm0.2)\times10^9$ dyn/cm^2 for the (110) stress]. For the following reasons we believe that the latter ones represent the true critical-stress values σ_{c1} and σ_{c2}. For the (110) stress, the stress value at the kink in γ_X [$\sigma_{c2} = (5.8\pm0.2)\times10^9$ dyn/cm^2] agrees with both the extrapolated vanishing point in γ_Z and the critical stress [$(5.4\pm0.2)\times10^9$ dyn/cm^2] deduced from Raman data discussed in Sec. V A (see Fig. 6). For the case of the (010) stress, the kink in γ_y coincides with the extrapolated vanishing point in the Raman data, which indicates a critical-stress value $\sigma_{c1} = (1.6\pm0.1)\times10^9$ dyn/cm^2. Further, as two types of domain with c axis perpendicular to the (010) stress may still remain, the result of the dielectric measurement along the direction in which the P_{s1} is developing (the measured "γ_x" curve) might be related to some average of γ_x and γ_z in Eqs. (12) or (15). Hence, the reported critical-stress value[18] (0.99×10^9 dyn/cm^2) should be discarded. (c) The linear characteristics above the critical stress observed for γ_y and γ_X are in accord with the theory which predicts that the deviation $\gamma_{\text{para}} - \gamma_{\text{ferro}}$ should be proportional to P_{si}^2 ($\propto \sigma - \sigma_{ci}$), though the magnitude of the deviation for γ_X seems to be a little larger than expected as compared with that of γ_y. The behavior of γ_Z above σ_{c2} also differs from the theoretical anticipation which expects a much steeper change above the transition stress. A similar phenomenon was observed also in the case of $KTaO_3$.[20] This might be ascribed to some mechanism due to the appearance of ferroelectric domains.

We now evaluate the electrostrictive coefficients $Q_{\lambda\mu}^t$ by comparing the values of the gradient $\partial\gamma_i/\partial\sigma$ observed below the transition stress with the corresponding equations in Sec. II B. From the observed γ_y and Eq. (12), we obtain $Q_{11}^t = (5.9\pm0.4)\times10^{-13}$ in cgs (henceforth we use these units). The observed values of $\gamma_a = 3.0\times10^{-4}$ cgs and $\sigma_{c1} = (1.6\pm0.2)\times10^9$ cyn/cm^2 give $Q_{12}^t = -\frac{1}{2}\gamma_a/\sigma_{c1} = (-0.94\pm0.07)\times10^{-13}$. From the gradient of γ_Z and Eq. (16), we get $Q_{13}^t = (-1.15\pm0.08)\times10^{-13}$. Using the data for γ_X and γ_Y and taking the values of Q_{11}^t and Q_{12}^t determined above, we obtain $Q_{66}^t = (2.1\pm0.6)\times10^{-13}$. Previously the measured value $Q_{13}^c = -1.26\times10^{-13}$ cgs at $T > T_a$, which nearly agrees with the present result, was reported.[26]

For the $t_{\lambda\mu}^X$ coefficients, we get from Eq. (8),

$$t_{11}^X - t_{12}^X = \tfrac{1}{2}(\gamma_a - \gamma_c)/\Phi_s^2 . \tag{25}$$

With the experimental values of γ_a, γ_c, and Φ_s,[35,36] $t_{11}^X - t_{12}^X = -1.10\times10^{15}$ cgs.[27] These values are reproduced in Table II.

V. RAMAN-SCATTERING EXPERIMENT AND DISCUSSION

A. Ferroelectric soft modes

This section deals with various aspects of a Raman-scattering experiment and the related discussion for the $SrTiO_3$ crystal. For technical reasons, the measurements were always done at about 2 K, whereas the dielectric constants were measured at 4.2 K, the variation of temperature being of no consequence for properties of the crystal in the liquid-He temperature region.

In the absence of external stress, the Raman spectra for the tetragonal $SrTiO_3$ are mostly due to either the second-order two-phonon modes[28] or the structural phonon modes that originate from R-point phonon modes above T_a and become Raman-active modes at the zone center below T_a.[2] The infrared-active FE soft modes are not observable in the paralectric phase, unless they are made Raman active by an external electric field.[10] Upon application of the mechanical stress with load higher than the critical stress, a new group of Raman lines corresponding to the FE soft modes emerges in the low-frequency region. An example of the

stress-induced change of Raman spectra is typically shown in Fig. 3. The weak line at 172 cm^{-1} in the figure is identified as due to the LO_1 or TO_2 modes which may be Raman-activated by the internal stress owing to some lattice defects. By comparing the two traces in the figure, the 172-cm^{-1} line will be seen not to change position with applied stress. The insensitivity to stress of the "hard" polar modes was generally confirmed also for the (110) stress. This fact validifies the assumption that only the lowest-frequency TO modes should vary with pressure following the LST relation. Characteristics of the FE modes are quite sensitive to the applied stress, as is clearly demonstrated for the $A_1(x)$ mode under the (010) stress in Fig. 4. In this figure, one notes that both the mode frequency and the line intensity increase and the line becomes sharper as the stress increases away from σ_{c1}.

In order to analyze the Raman profiles of the FE modes, we employ the damped-harmonic-oscillator model taking into account, however, the present condition that the observed spectra extend much higher than $kT \sim 2$ cm^{-1} [i.e., $n(\omega)+1 \sim 1$]. Then, the theoretical curve for the spectral density should take the form,

$$I(\omega) \propto \Gamma\omega/[(\omega^2 - \omega_0^2)^2 + \Gamma^2\omega^2] \ , \qquad (26)$$

where ω_0 is the undamped mode frequency and Γ is the damping constant that corresponds to the full width at half-maximum in the Lorentzian

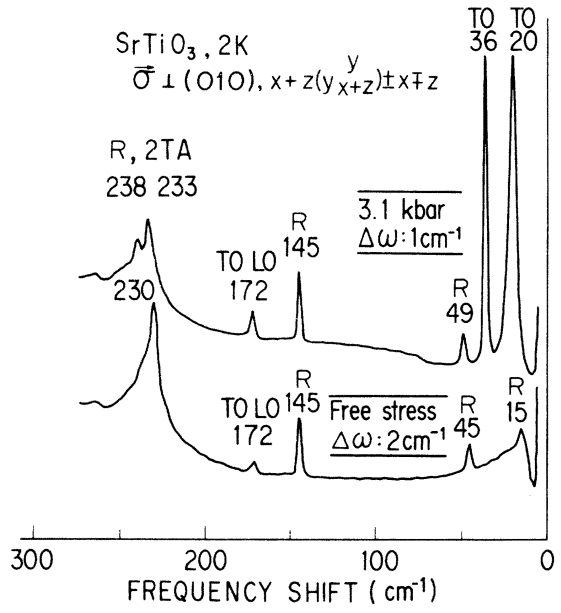

FIG. 3. Raman spectra of structural multidomain $SrTiO_3$ at 2 K under free or (010) stress, without analyzer. Symbol R in the figure denotes that the lines are due to the R-point structural modes.

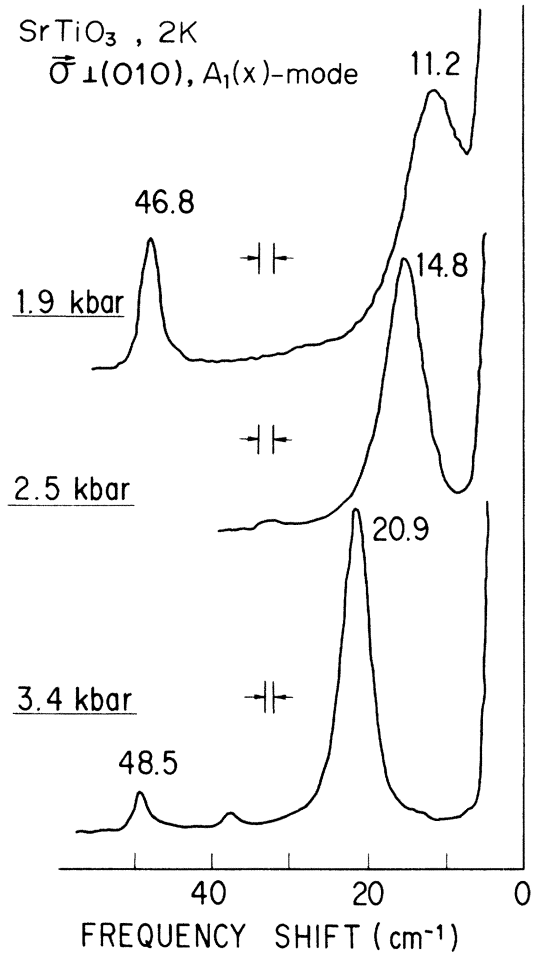

FIG. 4. Variation of the Raman spectra of the total symmetric ferroelectric mode as the applied (010) stress load approaches the critical stress (1.6 kbar).

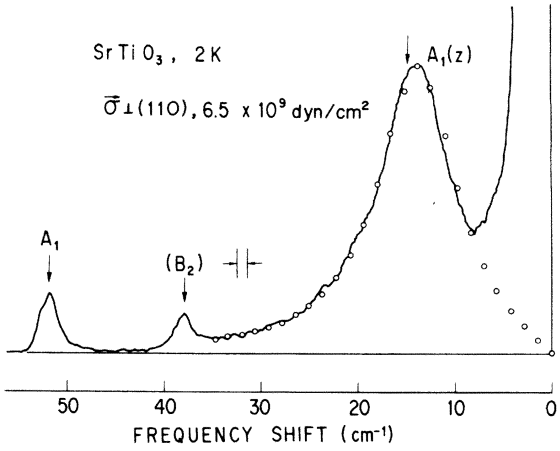

FIG. 5. Raman line shape for the ferroelectric $A_1(Z)$ mode under the (110) stress. The open circles are the results of the best fit of the theoretical curve [Eq. (26)] by adjusting ω_0 and Γ.

limit. It is worth noting that Eq. (26) predicts the spectral density curve with a peak even for the case of an overdamped mode at the classical limit $[n(\omega)+1 \sim kT/\hbar\omega]$. In the present experiment, however, the observed FE modes were found to always remain underdamped except very near the critical stresses (see Fig. 7). In Fig. 5 an example is shown for the case of (110) stress, where the Raman profile of the ferroelectric $A_1(Z)$ mode is fitted to Eq. (26). The open circles in the figure are the best fit of the theoretical curve by adjusting both ω_0 and Γ. We have applied this curve-fitting procedure to various phonon modes under the (010) or (110) stress. The results are summarized in Figs. 6 and 7. The square of the undamped phonon frequency ω_0^2 and the damping constant Γ thus obtained are plotted in these figures, respectively, as a function of the magnitude of the applied stress.

In Fig. 6 one may note that the linear relationship between ω_0^2 and σ holds for every FE mode observed. Measurements were always done for right-angle scattering with the observed phonon wave vector along the $\langle 100 \rangle$ direction. In this geometry, the $B_1(z)$ mode is forbidden by the Raman-tensor symmetry,[29] which is observed in the case of the oblique phonon, as described in Sec. V B. The transition stresses ($\sigma_{c1} = 1.6 \pm 0.1$ and $\sigma_{c2} = 5.4 \pm 0.2$ in units of 10^9 dyn/cm^2), defined as the vanishing points of the extrapolated lines of the total symmetric A_1 mode, are found to agree within experimental error with those of dielectric measurements. As the stress approaches the transition points, the Raman lines become broader and at the same time the integrated intensities of these modes decrease in rough proportion to $\sigma - \sigma_c$, so that an accurate determination of ω_0 and Γ could not be done in the vicinity of σ_c.

Below the critical stress, these polar FE modes become Raman forbidden and could not be observed in the present experiment. However, we can locate the positions of these modes in the paraelectric phase with the aid of the following relations that are derived from Eqs. (20), (21), and (23).

$$\Omega_P^2(E_u)_{\sigma=0}/\Omega_P^2(B_{2u})_{\sigma=\sigma_{c1}} = |Q_{12}^t|/(Q_{11}^t + |Q_{12}^t|), \tag{27a}$$

$$\Omega_P^2(A_{2u})_{\sigma=0}/\Omega_P^2(E_u)_{\sigma=0} = \gamma_c/\gamma_a, \tag{27b}$$

$$\frac{\partial\Omega^2(B_{3u}^{(010)})}{\partial\sigma} : \frac{\partial\Omega^2(B_{1u}^{(110)})}{\partial\sigma} : \frac{\partial\Omega^2(B_{2u}^{(110)})}{\partial\sigma} = 2Q_{12}^t : 2Q_{13}^t : Q_{11}^t + Q_{12}^t + \tfrac{1}{2}Q_{66}^t . \tag{27c}$$

By using the dielectric data described in Sec. IV, Eqs. (27) yield the theoretical curves shown as broken lines in Fig. 6, which seem to be consistent and reasonable. Consequently, the FE mode frequencies under free stress have to be $\Omega_P(E_u) = 9.1 \pm 0.6$ cm^{-1} and $\Omega_P(A_{2u}) = 19 \pm 1$ cm^{-1}. Previously, many investigations involving neutron inelastic scattering[9] and electric-field-induced Raman scattering[2,10] reported only one Cochran mode whose frequency lies around $\Omega_P(E_u)$. This appreciable splitting of the Cochran mode by the structural transformation has not been confirmed, nor has the existence of the A_{2u} mode been reported yet. A search by various means for the A_{2u} mode is desirable, though this mode will probably be relatively weak in intensity compared with the E_u mode.[30] Other aspects of the behavior of FE modes, such as the characteristics of the damping constant, etc., will be treated separately in the following subsections.

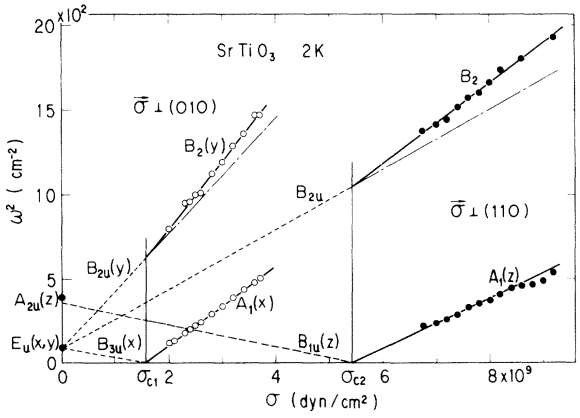

FIG. 6. Squared frequencies of the ferroelectric modes as a function of the (010) or (110) stress load. Broken lines below σ_{c1} and σ_{c2} are calculated ones using Eq. (27c) and the electrostrictive constants obtained from the dielectric measurements. Dots at $\sigma = 0$ are also theoretical ones using Eqs. (27a) and (27b).

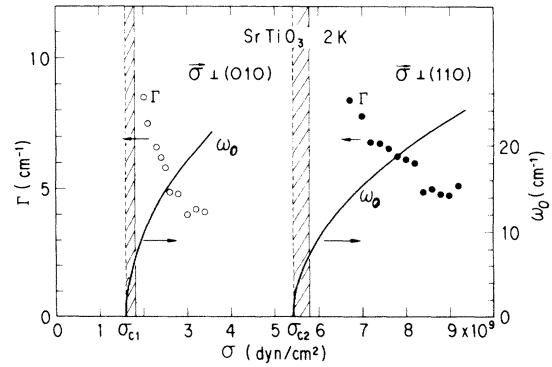

FIG. 7. Variations of the damping constant Γ and the undamped frequency ω_0 of the total symmetric FE mode as a function of stress load. Shaded parts near the critical stresses indicate the overdamped ($\Gamma > 2\omega_0$) region. For experimental points of ω_0 see Fig. 6.

B. Structural soft modes and the anticrossing phenomenon

In Figs. 8 and 9 are summarized data on the squared phonon frequencies of the structural soft modes as functions of (010) and (110) stresses, respectively. The linear relationship between ω_0^2 and σ is found to hold well for all R-point soft modes. At the respective transition points, however, no appreciable change was observed, which indicates that the contributions to Ω_Φ^2 from the term proportional to P_{si}^2, represented by the last terms in Eqs. (22) and (24), can be neglected. On the other hand, the observed gradients of $\partial\Omega_\Phi^2/\partial\sigma$ can give the information about the free-energy parameters $R_{\lambda\mu}$, as will be shown in Sec. V C.

We now turn to the anticrossing effect which is brought forth for the case of (010) stress and of phonon wave vector along the [101] direction. In this geometry, a ferroelectric $B_1(z)+A_1(x)$ mode is present, as depicted in the inset of Fig. 10. This hybridized oblique mode has been found to anticross with the structural $B_{2g}-B_1(z)$ mode, as demonstrated in Fig. 10. This behavior of the anticrossed branches is analyzed as follows. Let the amplitudes of the oblique FE mode and the structural mode denote, respectively, $(v/e^*)P$ and Φ_1. Then the kinetic-energy density T and the potential-energy density U are given by

$$T = \tfrac{1}{2}m_P(v/e^*)^2\dot{P}^2 + \tfrac{1}{2}m_\Phi\dot{\Phi}_1^2, \tag{28a}$$

$$U = \tfrac{1}{2}m_P(v/e^*)^2\Omega_{\rm obl}^2P^2 + \tfrac{1}{2}m_\Phi\Omega_\Phi^2(B_1)\Phi_1^2, \tag{28b}$$

where

$$\Omega_{\rm obl}^2 = \tfrac{1}{2}[\Omega_P^2(A_1(x)) + \Omega_P^2(B_1(z))].$$

The bilinear interaction $U_{\rm int}$ between P and Φ_1 is deduced from the Helmholtz free energy A [Eq. (1)]:

$$U_{\rm int} = \alpha P\Phi_1, \tag{28c}$$

where

$$\alpha = \left.\frac{\partial^2 A}{\partial\Phi_1\partial P}\right|_{\rm eq} = \frac{-t_{44}^x\Phi_s P_{s1}}{\sqrt{2}}.$$

By solving the equation of motion constructed from Eq. (28), one gets the expression of the coupled-mode frequencies,

$$\Omega_\pm^2 = \tfrac{1}{2}\left[\Omega_{\rm obl}^2 + \Omega_\Phi^2(B_1) \pm \left([\Omega_{\rm obl}^2 - \Omega_\Phi^2(B_1)]^2 + \frac{4(e^*/v)^2\alpha^2}{m_Pm_\Phi}\right)^{1/2}\right]. \tag{29}$$

Using the experimental curve for $\Omega_P(A_1(x))$ and the theoretical one for $\Omega_P(B_1(z))$, one can locate the $\Omega_{\rm obl}$ branch as shown by the broken line in Fig. 10. Here we assume that the increase of the

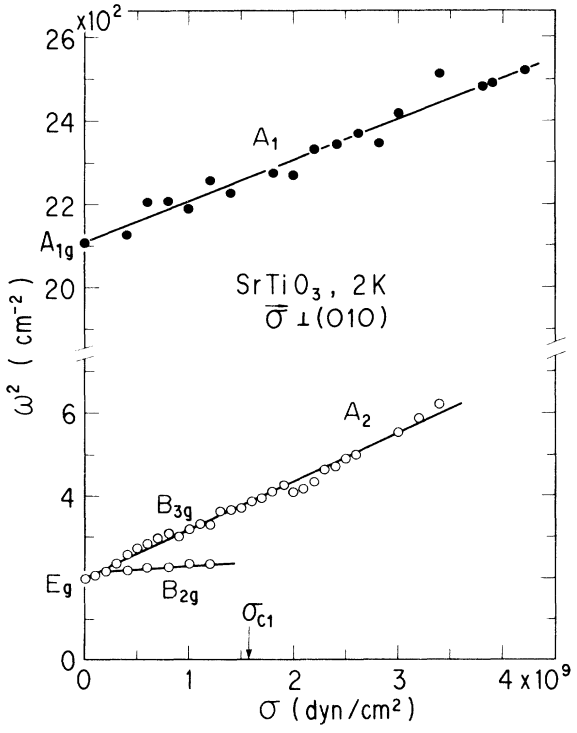

FIG. 8. Squared frequencies for the structural soft modes as a function of the (010) stress load.

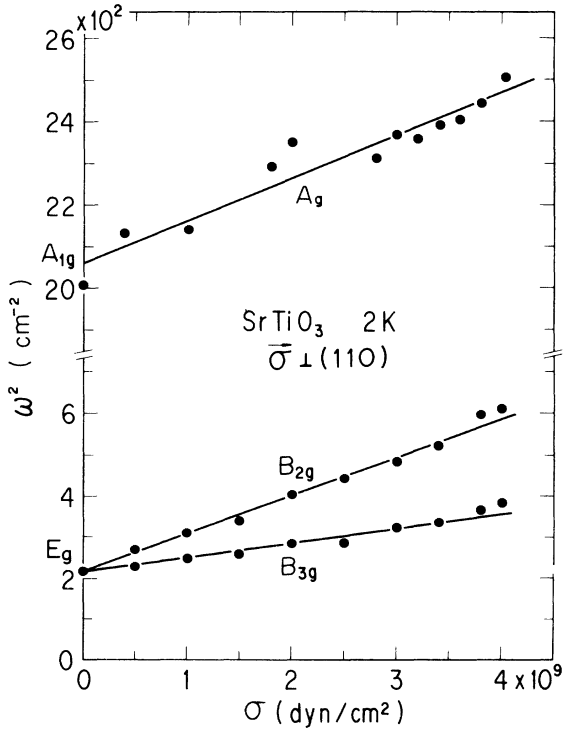

FIG. 9. Squared frequencies for the structural soft modes as a function of the (110) stress load.

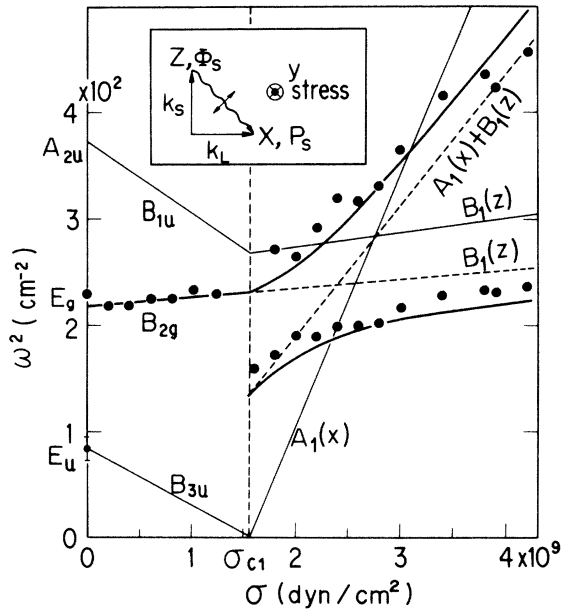

FIG. 10. Anticrossing of the ferroelectric $[A_1(x) + B_1(z)]$ and the structural $[B_1(z)]$ soft modes in the (010) stress-induced FE phase. Inset shows the Raman-scattering configuration.

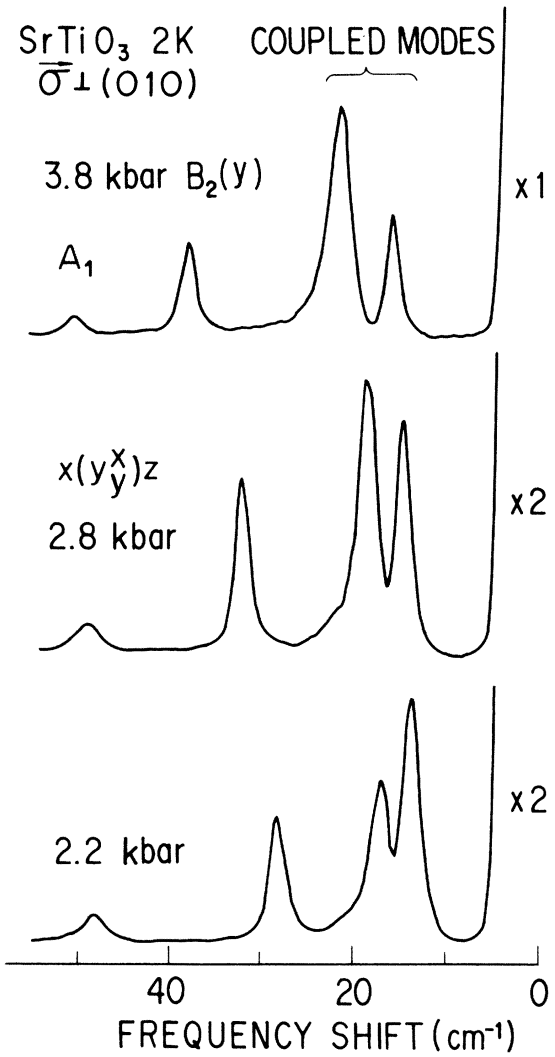

FIG. 11. Change of the Raman-line profiles of the coupled modes in the anticrossing stress region.

squared frequency in proportion to P_{s1}^2 for the $B_1(z)$ mode is nearly equal to that for the $B_2(y)$ mode [see Eq. (21)]. Then, through a curve-fitting procedure of the experimental data by adjusting α in Eq. (29), one obtains $\alpha^2/(\sigma - \sigma_{c1}) = 3.45\times10^{11}$ cgs. Figure 11 shows how Raman profiles of the coupled modes vary with stress. One can see that their relative intensities interchange as the stress traverses the anticrossing region $\sigma \simeq 2.8\times10^9$ dyn/cm^2. Since the intensity of the FE oblique mode will vary as $\sigma - \sigma_{c1}$ and that of the structural B_1 mode will stay constant but for the mutual interaction, this stress dependence in Fig. 11 can be understood only as a result of mode coupling. The anticrossing phenomenon can also be expected for the case of nonoblique FE modes, however, at higher stress load [~1.5×10^{10} dyn/cm^2 for the (010) stress and ~4×10^{10} dyn/cm^2 for the (110) stress] far from the region examined in the present study. The first observation of the anticrossing phenomenon in $SrTiO_3$ was previously reported by Fleury, Scott, and Worlock,[2] who employed electric field biasing to allow interaction of the different kind of soft modes. Our earlier report on the Raman spectra in pure $SrTiO_3$ should also be explained by the anticrossing effect.[31]

C. Evaluation of free-energy parameters

The coefficients $R_{\lambda\mu}$ appearing in the interaction terms $X_\lambda(\vec{\Phi}\vec{\Phi})_\mu$ of the free energy can be determined by analyzing the stress dependence of the structural mode frequencies shown in Figs. 8 and 9. For the (010) stress, we use Eq. (22), which gives

$$m_\Phi \frac{\partial \Omega^2_{\Phi_3}(A_g)}{\partial\sigma} = -4R_{12}\,,$$
$$m_\Phi \frac{\partial}{\partial\sigma}[\Omega^2_{\Phi_2}(B_{3g}) - \Omega^2_{\Phi_1}(B_{2g})] = 2(R_{11} - R_{12})\,, \tag{30}$$

where and henceforth we neglect the last terms involving P_{s1}^2. Then, taking $m_\Phi = 0.897$ g/cm^3,[17] the measured gradient values yield $R_{12} = -7.8 \pm 0.6$ and $R_{11} = 8.7 \pm 0.7$ in units of 10^{14} cgs. For the (110) stress, the following relations are derived from Eq. (24):

$$m_\Phi \frac{\partial \Omega^2_{\Phi_Z}(A_g)}{\partial \sigma} = -4\frac{A^x}{A^X}R_{12},$$

$$m_\Phi \frac{\partial}{\partial \sigma}[\Omega^2_{\Phi_X}(B_{2g}) + \Omega^2_{\Phi_Y}(B_{3g})] = 2R_{11} - R_{12}(2A^X + 2A^X_n + b^2_{44}/c_{44})/A^X, \quad (31)$$

$$m_\Phi \frac{\partial}{\partial \sigma}[\Omega^2_{\Phi_X}(B_{2g}) - \Omega^2_{\Phi_Y}(B_{3g})] = -R_{44}.$$

Then using the values of R_{11} and R_{12} obtained above, comparison with experimental data gives $R_{44} = (-1.84 \pm 0.15) \times 10^{15}$ cgs, $A^x/A^X = 1.19 \pm 0.26$, $(2A^X_n + b^2_{44}/c_{44})/A^X = 0.9 \pm 0.4$. The observed $\partial\Omega^2_\Phi/\partial\sigma$ for the $B_{2g} - B_1$ branch under (010) stress also gives $(2A^X_n + b^2_{44}/c_{44})/A^X = 1.1 \pm 0.6$, which thus furnishes evidence for the internal consistency of the analysis. Previously the B_{3g} mode for the (110) stress was observed at 8 K,[13] which result agrees with the present data. These $R_{\lambda\mu}$ values somewhat differ from those obtained by the biaxial-pressure study,[32] and also from those obtained from spontaneous-strain data.[33,34] However, in view of the characteristic that the lattice cell dimensions become nearly constant below about 50 K,[33] this discrepancy might be attributed to the difference in the measuring temperature.

We next determine the A coefficients. We adopt as the spontaneous value of the structural order parameter the value $\Phi_s = 6.89 \times 10^{-10}$ cm at 2 K previously obtained from ESR[35,36] and x-ray measurements.[33] Then, from the measured frequency $\Omega_\Phi(A_{1g})_{\sigma=0}$, the values of A^x and A^X are determined by using Eqs. (5) and (20). Further, A^x_n and A^X_n are derived from the value of $\Omega_\Phi(E_g)_{\sigma=0}$ in Eqs. (20) and (A1), $c_{\lambda\mu}$ and $b_{\lambda\mu}$ being known as reported below. The values of the coefficients thus obtained are also listed in Table II. The values of A^x/A^X and $(2A^X_n + b^2_{44}/c_{44})/A^X$ are calculated to be, respectively 1.1 and 0.81, which agree with the values obtained from those for $\partial\Omega^2_\Phi/\partial\sigma$. At the same time, we also get $\kappa_0 = -3.17 \times 10^{25}$ cgs. These A and κ_0 values agree fairly well with those cited in Ref. 17 (see Table II), in which the analysis is made under the assumption $b_{11} + 2b_{12} = 0$.

As was described in Sec. V A, the stress dependence of the FE modes has given information about the relative values of the electrostrictive coefficients $Q_{\lambda\mu}$ which proved to be consistent with dielectric data. Here we discuss the proportionality factor which contains the effective charge e^*. From Eqs. (12) and (21), we get

$$\frac{\partial \Omega^2_P(B_{3u})}{\partial \sigma} = 2\left(\frac{e^*}{v}\right)^2 m_P^{-1} Q^t_{12}. \quad (32)$$

Comparison of Eq. (32) with the observed gradient gives $(e^*/v)^2 m_P^{-1} = (1.0 \pm 0.2) \times 10^{28}$ cgs. Since the mass density for this mode[38] is evaluated as $m_P = 0.673$ g/cm^3, this results in $e^*/v = (8.1 \pm 0.8) \times 10^{13}$ cgs, which agrees with 8.23×10^{13} cgs from the infrared experiment.[37]

For the lateral $B_{2u} - B_2$ modes, let us consider the difference of the gradients

$$\Delta \equiv m_P \left(\frac{v}{e^*}\right)^2 \left[\left(\frac{\partial \Omega^2_P}{\partial \sigma}\right)_{\sigma > \sigma_c} - \left(\frac{\partial \Omega^2_P}{\partial \sigma}\right)_{\sigma < \sigma_c}\right]$$

From Eqs. (21) and (23), we get

$$\Delta^{(010)} = -2Q^t_{12}\left(1 + \frac{D^X_n + g^2_{44}/2c_{44}}{2[D^X - (t^X_{12})^2/4A^X]}\right),$$

$$\Delta^{(110)} = -2Q^t_{13}\left(1 + \frac{D^X_n + g^2_{44}/2c_{44} - t^X_{12}(t^X_{11} - t^X_{12})/2A^X}{2[D^X - (t^X_{12})^2/4A^X]}\right). \quad (33)$$

The experimental value is $\Delta^{(010)} \sim \Delta^{(110)} \sim 2.0 \times 10^{-13}$ cgs, which nearly agrees with the value of $-2Q^t_{12}$ or $-2Q^t_{13}$. This result indicates that the anisotropic quartic term of P in the free energy should be considerably small compared with the spherical term, which is consistent with the behavior of the FE mode under the electric field[10] (in the notation of Ref. 10, $\xi = \xi'$).

For the total symmetric FE mode, the ratio of the gradients above and below σ_c should follow the equation

$$\frac{(\partial \Omega^2_P/\partial \sigma)_{\sigma > \sigma_c}}{(\partial \Omega^2_P/\partial \sigma)_{\sigma < \sigma_c}} = 2D^x/[D^X - (t^X_{12})^2/4A^X], \quad (34)$$

for the (010) stress. A similar equation holds for the (110) stress, replacing t_{12} by t_{11}. The observed ratios were found to be 4.50 ± 0.62 and 2.04 ± 0.4 for (010) and (110) stresses, respectively. This indicates that the correction terms involving t^X_{11} or t^X_{12} are not negligible. In fact, $(t^X_{12})^2/4A^X$ will amount to $\sim 5 \times 10^{-13}$ cgs assuming $t^X_{12} \sim 10^{15}$ cgs, which is the same order of magnitude of D^X reported previously.[10]

The value of the spontaneous polarization in the ferroelectric phase might be estimated from the observed frequencies of the total symmetric FE mode. Equations (21) and (23) indicate that the squared frequencies should vary as $D^x P^2_{si}$ above σ_{ci}. Hence, one needs to know the value of D^x. Accurate information for D^x is difficult to obtain, since previous reports give rather scattered data without taking the dielectric anisotropy into account. When we adopt the value $D^x = (2-5) \times 10^{-12}$ cgs,[39] this gives $P_{s1} = 2-4$ μC/cm^2 at a stress 2 kbar higher than σ_{c1}. This value is one order of magnitude larger than the experimental value of the D-E hysteresis observation.[40]

The coupling parameters $g_{\lambda\mu}$ and $b_{\lambda\mu}$ can be calculated from $Q_{\lambda\mu}$ and $R_{\lambda\mu}$ using relations (A2) and (A3), where data on elastic constants are needed.

TABLE II. Parameters for $SrTiO_3$ at liquid-He temperature.

	Present work	Slonczewski and Thomas [a]	Bruce and Cowley [b]	Units
Q_{11}^t	5.9		17	10^{-13} cgs
Q_{12}^t	−0.94			
Q_{13}^t	−1.15		−6.3	
Q_{66}^t	2.1			
g_{11}	1.48			cgs
g_{12}	0.36			
g_{44}	0.27			
R_{11}	8.7			10^{14} cgs
R_{12}	−7.8			
R_{44}	−18.4			
b_{11}	1.3	3.36	1.76	10^{27} cgs
b_{12}	−2.5	−1.68	−1.84	
b_{44}	−2.3	−2.51	−1.76	
$t_{11}^X - t_{12}^X$	−1.10			10^{15} cgs
$\lvert t_{44}^x \rvert$	5–9			
A^x	1.94	1.95	1.4	10^{43} cgs
A^X	1.67	1.58		
A_n^x	0.08	−0.24	0.04	
A_n^X	0.49	0.62		
κ_0	−3.17	−3.08		10^{25} cgs
e^*/v	8.1			10^{13} cgs
m_P	0.673			g/cm^3
m_Φ	0.897			

[a] References 22 and 17.
[b] Reference 41.

We take $c_{11} = 3.36 \times 10^{12}$, $c_{12} = 1.07 \times 10^{12}$, and $c_{44} = 1.27 \times 10^{12}$ cgs, which are estimated from the values observed in the cubic phase by extrapolating them to liquid-helium temperature using the empirical formulas in Ref. 26.[17] The t_{44}^x value can be estimated from the measured value of the coupling constant α (see Sec. V B) between the FE and structural modes, by using the above-mentioned P_{s1} and Φ_s values.[35,36] The calculated values are listed in Table II.

In passing, let us briefly comment on the relative magnitudes of the coefficients $b_{\lambda\mu}$ and $g_{\lambda\mu}$ which represent couplings of Φ_i and P_i, respectively, with the lattice strain x_μ. Experimental observations have shown that $b_{11} \ll |b_{12}|$, $|b_{44}|$ and $g_{11} \gg g_{12}, g_{44}$. Let us recall that the structural order parameter Φ_i stands for the mode pattern in which the displacements of the atoms are confined to the plane perpendicular to the rotation axes (in this case, the 1 axis) of oxygen octahedra. In contrast, the ferroelectric order parameter P_i is known to be the Slater mode[38] in which the relative displacements of the atom are confined along the polar axis. Hence, it seems probable that the structural soft mode strongly couples with the lattice strain in the 2-3 plane, whereas the ferroelectric mode couples with the lattice strain along the 1 axis. Therefore the dominance

of b_{12} and g_{11} over b_{11} and g_{12} is quite understandable.

In Table II are also cited values of parameters estimated by Bruce and Cowley,[41] based on the anharmonic-lattice-dynamical model, together with those previously given by Slonczewski and Thomas.[17,22] It is especially to be noted that the theoretical condition $b_{11} = -b_{44}$ does not seem to hold in the present results. This may probably suggest that (a) the noncentral Ti-O and Sr-O interactions are important, and/or (b) the O-O and Ti-Sr interactions should not be negligible.

D. Divergence of damping constant

It was experimentally observed that the damping constant of the ferroelectric A_1 modes is quite sensitive to the applied stress. In Fig. 7 it is shown how the damping constant Γ and the corresponding phonon frequencies vary with the stress. As the stress approaches the critical stress, the Γ value of each mode was found to increase hyperbolically, while the phonon frequency decreases toward zero value. As can be seen in Fig. 7, however, the phonon modes always remain *underdamped* over the measured stress region. The observed linewidth can probably be regarded as the homogeneous one, because (a) the Raman line shape can always be fitted to the theoretical curve of Eq. (26): (b) the sampling volume for the Raman observation is quite small as described in Sec. III.

Previously, the divergent nature of the damping constant for the FE mode was reported in the cases of[42] $PbTiO_3$ and[43] $Gd_2(MoO_4)_3$, and was denied in the case of the structural phase transition of $SrTiO_3$.[44] At any rate, the theoretical interpretation of this phenomenon does not seem to be known, at least it is not settled, yet, as will be briefly reviewed below. Tani developed his theory of the lifetime of the soft phonon mode for the one-dimensional case,[45] and Pytte also treated this problem using the Green's function.[46] Dvořák calculated the lifetime owing to the $TO(k=0) + TA \rightarrow TO(k \neq 0)$ process,[47] and Silverman proposed a $TO(k=0) + TA \rightarrow LA$ process.[48] However, in the low-temperature range we are concerned with at present, as the thermal excitation of TA phonons is expected to be negligibly small, the relaxation mechanism in which the above TA phonons participate should be regarded as rather ineffective. Barrett pointed out that the $TO(k=0) \rightarrow TA + LA$ process might be the dominant relaxation precess for stress-free $SrTiO_3$ and $KTaO_3$ crystals at lower temperatures.[49] Furthermore, Nettleton argued that the three-phonon process involving the TA phonon could give, at best, a contribution of $O(\omega_0)$ to the inverse lifetime of the TO phonon mode, because this process can scatter wave vectors only in a thin shell in k space.[50] Hence, it seems almost impossible to explain the divergent damping constant in the stressed $SrTiO_3$ by a theory based on the three-phonon process. Nettleton evoked a four-phonon process to analyze the thermal conductivity of $SrTiO_3$,[50] though this scheme does not explain the divergent nature of the damping constant of the TO mode near $k=0$. Bruce and Cowley[41] calculated the linewidth of the FE modes in $SrTiO_3$ and $BaTiO_3$, employing the anharmonic parameters based on their lattice-dynamical model, and they could explain the temperature dependence of the linewidth in these cases. However, the interaction terms in the Hamiltonian, which consist of three- and four-phonon processes, might not give a divergent Γ for the present case of the $PbTiO_3$ crystal. In conclusion, the problem should perhaps be ascribed to the more-than-four-phonon process or to some other mechanism to be considered from a different viewpoint.

VI. SUMMARY

In order to understand stress-induced ferroelectricity in $SrTiO_3$, we have done experiments including measurements of dielectric constants, and Raman-scattering experiments under uniaxial (010) or (110) stress at liquid helium temperatures, results of which have been analyzed by using Landau-Devonshire-type phenomenological theory. In the following we summarize the obtained results. (a) From the free energy of the crystal, which contains as arguments the electric polarization, the staggered rotation of the oxygen octahedra, and the homogeneous strain, and also their mutual-interaction terms, theoretical forms of the physical quantities involving the dielectric constant and the frequencies of the ferroelectric and structural soft modes have been derived as a function of the stress. (b) The inverse dielectric susceptibilities have been found to change linearly with stress. (c) One of the components of the dielectric constant has been found to increase divergently as the stress approaches the critical value. (d) By means of Raman-scattering measurements, the ferroelectric soft modes have been observed above the critical stress. Their frequencies have been found to change concurrently with the behavior of the dielectric constants following the LST relation. The frequency of the total symmetric FE mode has been found to become vanishingly small as the stress approaches the critical value. (e) Frequencies of structural soft modes have been found to exhibit remarkable stress dependences. (f) The anticrossing phenomenon between the ferroelectric and structrual

soft modes has been observed in the stress-induced ferroelectric phase, which has been explained by the coupled-mode formulation derived from the free energy. (g) By comparing the experimental results with the phenomenological theory, the respective parameters involved in the free energy have been consistently determined. (h) An anomalous increase of the damping constant of the ferroelectric soft mode near the critical stress has been observed. This phenomenon is discussed in connection with existing theories.

ACKNOWLEDGMENTS

The authours would like to thank H. Unoki and Y. Fujii for many stimulating discussions.

APPENDIX

(i) When one uses the contracted notation for the suffices of the quartic terms in the free energy, care must be taken to avoid confusion about the multiplication factor 2.[23] The fourth rank tensors in A and G^c are converted to those of matrix notation by the following relations:

$$c_{1111}=c_{11},\quad c_{1122}=c_{12},\quad c_{2323}=c_{44},$$
$$g_{1111}=g_{11},\quad g_{1122}=g_{12},\quad 2g_{2323}=g_{44},$$
$$b_{1111}=b_{11},\quad b_{1122}=b_{12},\quad 2b_{2323}=b_{44},$$
$$t^x_{1111}=t^x_{11},\quad t^x_{1122}=t^x_{12},\quad 4t^x_{2323}=t^x_{44},\ \ldots,$$

and

$$Q^c_{1111}=Q^c_{11},\quad Q^c_{1122}=Q^c_{12},\quad 4Q^c_{2323}=Q^c_{44},$$
$$R_{1111}=R_{11},\quad R_{1122}=R_{12},\quad 4R_{2323}=R_{44}.$$

For instance, the interaction term involving $g_{\lambda\mu}$ in A goes as

$$-g_{11}(x_1P_1^2+x_2P_2^2+x_3P_3^2),$$
$$-g_{12}[x_1(P_2^2+P_3^2)+x_2(P_3^2+P_1^2)+x_3(P_1^2+P_2^2)],$$
$$-g_{44}(x_4P_2P_3+x_5P_3P_1+x_6P_1P_2).$$

(ii) The symbols appearing in G^c are connected with those of A by the following relations:

$$\begin{aligned}
&D^X=D^x-(g_{11}+2g_{12})^2/6(c_{11}+2c_{12})-(g_{11}-g_{12})^2/3(c_{11}-c_{12}),\\
&D^X_n=D^x_n+(g_{11}-g_{12})^2/(c_{11}-c_{12})-g_{44}^2/2c_{44},\\
&A^X=A^x-(b_{11}+2b_{12})^2/6(c_{11}+2c_{12})-(b_{11}-b_{12})^2/3(c_{11}-c_{12}),\\
&A^X_n=A^x_n+(b_{11}-b_{12})^2/(c_{11}-c_{12})-b_{44}^2/2c_{44}.
\end{aligned}\tag{A1}$$

$$\begin{aligned}
&Q^c_{11}=(g_{11}+2g_{12})/3(c_{11}+2c_{12})+2(g_{11}-g_{12})/3(c_{11}-c_{12}),\\
&Q^c_{12}=(g_{11}+2g_{12})/3(c_{11}+2c_{12})-(g_{11}-g_{12})/3(c_{11}-c_{12}),\\
&Q^c_{44}=g_{44}/c_{44}.
\end{aligned}\tag{A2}$$

$$\begin{aligned}
&R_{11}=(b_{11}+2b_{12})/3(c_{11}+2c_{12})+2(b_{11}-b_{12})/3(c_{11}-c_{12}),\\
&R_{12}=(b_{11}+2b_{12})/3(c_{11}+2c_{12})-(b_{11}-b_{12})/3(c_{11}-c_{12}),\\
&R_{44}=b_{44}/c_{44}.
\end{aligned}\tag{A3}$$

$$\begin{aligned}
&t^X_{11}=t^x_{11}+g_{11}R_{11}+2g_{12}R_{12},\\
&t^X_{12}=t^x_{12}+g_{11}R_{12}+g_{12}R_{11},\\
&t^X_{44}=t^x_{44}+g_{44}R_{44}.
\end{aligned}\tag{A4}$$

Note added in proof. After this paper was submitted for publication, the following paper appeared: D. Heinman, S. Ushioda, and J. P. Remeika, Phys. Rev. Lett. 34, 886 (1975). By using a polariton-scattering technique, they found increase of the damping constant for the FE mode of $PbTiO_3$ as the polariton frequency was decreased at room temperature. The attributed this anomalous damping to the process of TO ($k=0$) + TA (zone boundary) − LA (zone boundary), which can not, however, be applied to our cases in $SrTiO_3$, because TA-zone-boundary phonons are not excited in the temperature range as low as 2 K.

*Based on work submitted to the University of Tokyo in partial fulfillment of the requirements for the Doctor of Science degree.

[1]H. Unoki and T. Sakudo, J. Phys. Soc. Jpn. 23, 546 (1967).

[2]P. A. Fleury, J. F. Scott, and J. M. Worlock, Phys. Rev. Lett. 21, 16 (1968).

[3]G. Shirane and Y. Yamada, Phys. Rev. 177, 858 (1969).

[4]H. Thomas and K. A. Müller, Phys. Rev. Lett. 21, 1256 (1968).
[5]H. E. Weaver, J. Phys. Chem. Solids 11, 274 (1959).
[6]T. Sakudo and H. Unoki, Phys. Rev. Lett. 26, 851 (1971).
[7]J. H. Barrett, Phys. Rev. 86, 118 (1952).
[8]B. D. Silverman and R. I. Joseph, Phys. Rev. 129, 2062 (1963).
[9]Y. Yamada and G. Shirane, J. Phys. Soc. Jpn. 26, 396 (1969).
[10]P. A. Fleury and J. M. Worlock, Phys. Rev. 174, 613 (1968).
[11]For the hydrostatic-pressure effect on phase transitions in $SrTiO_3$, see G. A. Samara, Ferroelectrics 2, 177 (1971); G. Sorge, G. Schmidt, E. Hegenbarth, and G. H. Frenzel, Phys. Status Solidi K 37, 17 (1970).
[12]W. J. Burke and R. J. Pressley, Solid State Commun. 7, 1187 (1969).
[13]W. J. Burke, R. J. Pressley, and J. C. Slonczewski, Solid State Commun. 9, 121 (1971).
[14]T. S. Chang, J. F. Holzrichter, G. F. Imbush, and A. L. Schawlow, Solid State Commun. 8, 1179 (1970).
[15]M. Rokni and L. S. Wall, J. Chem. Phys. 55, 435 (1971).
[16]K. A. Müller, W. Berlinger, and J. C. Slonczewski, Phys. Rev. Lett. 25, 734 (1970).
[17]J. C. Slonczewski, Phys. Rev. B 2, 4646 (1970).
[18]W. J. Burke and R. J. Pressley, Solid State Commun. 9, 191 (1971).
[19]Y. Fujii, H. Uwe, H. Unoki, and T. Sakudo, Acta Crystallogr. A 28, S230 (1970).
[20]H. Uwe, H. Unoki, Y. Fujii and T. Sakudo, Solid State Commun. 13, 737 (1973).
[21]H. Uwe and T. Sakudo, J. Phys. Soc. Jpn. 38, 183 (1975).
[22]J. C. Slonczewski and H. Thomas, Phys. Rev. B 1, 3599 (1970).
[23]J. F. Nye, *Physical Properties of Crystals* (Claredon, Oxford, 1960).
[24]K. A. Müller, W. Berlinger, M. Capizzi, and M. Gränicher, Solid State Commun. 8, 549 (1970).
[25]T. S. Chang, J. F. Holzrichter, G. F. Imbush, and A. L. Schawlow, Appl. Phys. Lett. 17, 254 (1970).
[26]R. O. Bell and G. Rupprecht, Phys. Rev. 129, 90 (1963).
[27]This value can also be determined from the values of Q_{12}^t and Q_{13}^t. Since the difference of these values is small, the above value determined from the dielectric constant should be regarded as more reliable.
[28]W. G. Nilsen and J. G. Skinner, J. Chem. Phys. 48, 2240 (1968).
[29]R. Loudon, Adv. Phys. 13, 423 (1964).
[30]In the electric-field-induced Raman-scattering experiments (Refs. 2 and 10) the scattered phonon was directed along the pseudocubic [110] direction. Taking account of the three possible structural c axes, the number of scattering events for the transverse A_{2u}, E_u, and oblique $A_{2u}+E_u$ phonons is estimated to be in the ratio 1:3:2. In the neutron-scattering experiment (Ref. 9), the scattering intensity for the A_{2u} mode might be weaker than that for the E_u mode, because the energy of the former is higher than that of the latter phonon. In addition, the ratio of the scattering events for the A_{2u} and E_u phonons can be estimated as 1:2 for the [100] propagation direction of the phonon.
[31]T. Sakudo and H. Uwe, Ferroelectrics 8, 587 (1974).
[32]K. Fossheim and B. Berre, Phys. Rev. B 5, 3292 (1972).
[33]A. Okazaki and M. Kawaminami, Mater. Res. Bull. 8, 545 (1973).
[34]From data of the spontaneous strain (Ref. 33) and Φ_S value (Refs. 35 and 36) near T_a, one gets $R_{11}=12.3$ and $R_{12}=-9.7$ in units of 10^{14} cgs. From the (111) stress dependence of the structural mode frequency (Ref. 15), $R_{44}=-3\times10^{15}$ cgs. These $R_{\lambda\mu}$ values and Eq. (A1) lead to $b_{11}=2.07$, $b_{12}=-2.95$, and $b_{44}=-0.10$ in units of 10^{27} cgs. From the biaxial pressure study (Ref. 32), $b_{11}=1.87$ and $b_{12}=-1.08$ in units of 10^{27} cgs.
[35]H. Unoki and T. Sakudo, Phys. Lett. A 32, 368 (1970).
[36]K. A. Müller, W. Berlinger, and F. Waldner, Phys. Rev. Lett. 21, 814 (1968).
[37]A. S. Barker, Jr., Phys. Rev. 145, 391 (1966).
[38]J. Harada, J. D. Axe, and G. Shirane, Acta Crystallogr. A 26, 608 (1970).
[39]These values are taken from Ref. 10 and other references therein. The more recent experiment is reported by B. Pietrass and H. Hegenbarth [J. Low Temp. Phys. 7, 201 (1971).
[40]In Ref. 18, the P_{S1} value was measured below $\sigma=1.7\times10^9$ dyn/cm^2, and was reported as 0.35 μC/cm^2 at the maximum stress load. From an ESR experiment [T. Waldkirch and K. A. Müller, Helv. Phys. Acta 46, 331 (1973)], the upper bound value of 0.5 μC/cm^2 at 1.5×10^9 dyn/cm^2 was extracted. Since these measurements were done just above or below the critical stress (1.6×10^9 dyn/cm^2) determined in the present work, experiments at much larger stress load than the critical stress are needed for the direct estimate of the spontaneous polarization.
[41]A. D. Bruce and R. A. Cowley, J. Phys. C 6, 2422 (1973).
[42]G. Burns and B. A. Scott, Phys. Rev. Lett. 25, 167 (1970); G. Burns, Phys. Rev. B 10, 1951 (1974).
[43]P. A. Fleury, Solid State Commun. 8, 610 (1970).
[44]E. F. Steigmeier and H. Auderset, Solid State Commun. 12, 565 (1973).
[45]K. Tani, J. Phys. Soc. Jpn. 26, 93 (1969).
[46]E. Pytte, Phys. Rev. B 1, 924 (1970).
[47]V. Dvořák, Czech. J. Phys. B 17, 726 (1967).
[48]B. D. Silverman, Solid State Commun. 10, 377 (1972).
[49]H. H. Barrett, Phys. Rev. 178, 743 (1968).
[50]R. E. Nettleton, Phys. Rev. 140, A1453 (1965).